

STRUCTURE AND ELECTROCHEMICAL PROPERTIES OF CARBON NANOTUBES SYNTHESIZED WITH CATALYSTS OBTAINED BY DECOMPOSITION OF Co, Ni, AND Fe POLYOXOMOLYBDATES SUPPORTED BY MgO

E. V. Lobiak¹, L. G. Bulusheva^{1,2}, A. A. Galitsky¹,
D. A. Smirnov⁴, E. Flahaut³, and A. V. Okotrub^{1,2}

Carbon nanotubes (CNTs) were synthesized by thermal decomposition of methane at 900 °C using Co–Mo/MgO, Fe–Mo/MgO, and Ni–Mo/MgO catalysts. To obtain metallic nanoparticles, polyoxomolybdate clusters of Co, Ni, and Fe deposited on MgO were thermally decomposed at 700 °C, and the obtained oxides were heated in a carbon-containing atmosphere. The method of transmission electron microscopy (TEM) testified formation of one to ten walled CNTs with the average outer diameter depending on the catalyst used. Raman spectroscopy data confirmed the presence of single-walled CNTs in the samples obtained with Co–Mo/MgO and Fe–Mo/MgO catalysts. The electrochemical properties demonstrated by the obtained materials in supercapacitors are shown to be functions of their structural and compositional features.

DOI: 10.1134/S0022476618040066

Keywords: carbon nanotubes, CCVD synthesis, polyoxomolybdates of Co, Ni, Fe, supercapacitor.

INTRODUCTION

As a multiparameter process, the method of catalytic chemical vapor deposition (CCVD) is widely used to grow carbon nanotubes (CNTs) of various structures. The decomposition of carbon-containing molecules and the growth of CNTs imply catalysts, which play the key role in this method [1]. Commonly used catalysts are iron-subgroup metals such as Fe [2, 3], Ni [4], and Co [5]. The diameter of CNTs is affected by the size of catalytic particles, therefore, the catalysts are deposited on the oxides possessing high surface areas to stabilize small particles. Magnesium oxide (MgO) is one such popular catalyst support which can be easily removed from the product of the synthesis by dilute hydrochloric acid. In particular, the Co/MgO catalyst allows obtaining thin (including single-walled) CNTs, depending on the temperature of carbonation in the atmosphere of methane [6].

Adding refractory metals such as Mo and W is another way to limit the size and preserve the structure of catalytic particles under high-temperature CCVD conditions [7-9]. It was shown that combining Fe or Co with Mo affects the number

¹Nikolaev Institute of Inorganic Chemistry of SB RAS, Novosibirsk, Russia; lobiakov@niic.sbras.ru. ²Novosibirsk State University, Novosibirsk, Russia. ³CNRS, Institut Carnot Cirimat, F-31062 Toulouse, France. ⁴Institute of Solid State Physics, Dresden University of Technology, 01062 Dresden, Germany. Translated from *Zhurnal Strukturnoi Khimii*, Vol. 59, No. 4, pp. 820-826, May-June, 2018. Original article submitted December 25, 2017.

of CNTs walls, their degree of graphitization, outer diameter, and the yield [10, 11]. A cluster compound containing Co and W was used as a source of catalytic nanoparticles to grow single-walled CNTs of certain chirality [12]. The structure of CNTs depends not only on the composition of the catalyst [13-15], but also on the method of its activation. Harutyunyan et al. studied the synthesis of CNTs from methane using Fe and FeMo particles and demonstrated the necessity of reducing Fe particles to activate the catalyst [16].

In this work, we present a method of CNT synthesis as a result of thermal decomposition of methane in the conditions of non-constant temperature profile using the catalysts formed by Co, Ni, and Fe polyoxomolybdates deposited on MgO. Using such a profile, Flahaut et al. could selectively grow double-walled CNTs on a Co–Mo/MgO catalyst prepared by the method of flash combustion [17]. The aim of our study is to establish how the nature of the active metal affects the CNT structure and to determine the relationship between structural parameters of the material and its electrochemical behavior in supercapacitors. Carbon nanomaterials are high in demand in the field of energy storage, and their effectiveness depends on their structure [18]. The obtained samples were characterized by the methods of scanning electron microscopy (SEM), transmission electron microscopy (TEM), near edge X-ray absorption fine structure spectroscopy (NEXAFS), and Raman spectroscopy. The electrochemical properties were studied with the method of cyclic voltammetry (CV) using an aqueous 1M H₂SO₄ solution.

EXPERIMENTAL

Synthesis. Polyoxomolybdates Mo₁₂O₂₈(μ₂-OH)₁₂{Ni(H₂O)₃}₄, Mo₁₂O₂₈(μ₂-OH)₁₂{Co(H₂O)₃}₄, and [H₄Mo₇₂Fe₃₀O₂₅₄(CH₃COO)₁₀{Mo₂O₇(H₂O)}{H₂Mo₂O₈(H₂O)}₃(H₂O)₈₇] were synthesized according to customary techniques [19, 20]. An aqueous suspension of MgO and a polyoxomolybdate was stirred at 60 °C until the water was totally evaporated. The precipitate was dried at 80 °C for 24 h to obtain beige, peach-orange, and light orange powders for {Ni₄Mo₁₂}, {Co₄Mo₁₂}, and {Fe₃₀Mo₇₂} clusters, respectively. According to the atomic emission spectroscopy data (iCAP- 6500 spectrometer), the content of Ni, Co, and Fe metals was about 1 wt.%.

Activation of the catalyst and CCVD synthesis of CNTs were carried out in a horizontal tubular reactor having the diameter of 7 cm, the length of 1.6 m, and a 15 cm zone of constant temperature. {Ni₄Mo₁₂}/MgO, {Co₄Mo₁₂}/MgO, and {Fe₃₀Mo₇₂}/MgO powders were precalcined in a muffle at 700 °C for 10 min. The resulting gray products were uniformly distributed in a ceramic boat in the central zone of the CCVD reactor. The gas mixture of CH₄ (67.5 ml/min) and H₂ (307.5 ml/min) was supplied to the reactor throughout the synthesis starting from the ambient temperature, then heated to the required temperature, and finally cooled in the reactor to 120 °C. Fig. 1 shows the temperature profile of the synthesis. The heating rate was 5 deg/min. After reaching 900 °C, the temperature was kept constant for 6 min, and then the heating was switched off to make the reactor cool down naturally. After cooling to 120 °C, the reactor was blown by N₂ for one hour. MgO and the metals were removed from the products of CCVD synthesis using dilute hydrochloric acid.

Instrumental methods. SEM and TEM images of the samples were obtained on JEOL JSM-6700F and JEOL-2010 microscopes, respectively. Raman spectra were recorded on a HORIBA “LabRAM HR Evolution” spectrometer with a 633 nm Ar⁺ laser. The specific surface of the samples was measured on a “Sorbometr-3.1” system. Nitrogen was used as the working gas environment, the measurement error was ±0.06. NEXAFS C K-edge spectra were recorded by measuring the

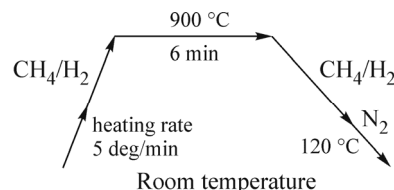


Fig. 1. Temperature profile of CCVD synthesis of CNTs.

total quantum yield of the electrons at the BESSY II synchrotron radiation source (Berlin) using the equipment of the Russian-German beamline. The energy resolution of the monochromator was \sim 80 meV. The normalizing spectrum of the incident emission was measured using the electrical signal from a gold grid placed in front of the sample. The intensities of NEXAFS spectra were normalized to the peak of the σ^* -resonance.

Electrochemical properties of obtained materials were studied in a three-electrode cell. The working electrodes were prepared by mixing \sim 5 mg of the sample and 1 μ l of a 62% “Teflon F-4D” solution to obtain a homogeneous mass which was further rolled into thin films. An Ag/AgCl electrode was used as a reference electrode. Platinum foil was used as a counter electrode and a current collector. The working electrode and the counter electrode were separated by a nonwoven polypropylene fiber impregnated by an aqueous 1M H₂SO₄ solution. The CV curves were recorded on the Elins P-30s potentiostat at 0-1 V with the scan rate of 2-1000 mV/s. The specific capacitance (C) of the electrode was determined as $C = A/(Vs \cdot m)$, where A is the square of the positive curve, Vs is the scan rate, and m is the mass of the carbon nanomaterial.

RESULTS AND DISCUSSION

Structure of materials. According to X-ray diffraction (XRD) data, the polyoxomolybdates decompose in air to form NiMoO₄, CoMoO₄, and Fe₂(MoO₄)₃ compounds which are reduced at 900 °C in the atmosphere of H₂ to the phases isostructural with Co₃Mo₃N, Ni₃Mo₃N [21], and Fe₃Mo [22]. According to the energy-dispersive X-ray spectroscopy data, the metal alloys of CoMo and NiMo are approximately in a 1:1 ratio inside the cavities of multi-walled CNTs (MWNTs) synthesized with Co–Mo/MgO and Ni–Mo/MgO catalysts.

Fig. 2a, b, c shows representative SEM images of carbon materials obtained with Fe–Mo/MgO, Ni–Mo/MgO, and Co–Mo/MgO catalysts. Individual CNTs are clearly seen against the loose felt-like material (Fig. 2a). The obtained TEM data indicate that this material is composed of intertwined CNTs (Fig. 3a). High-resolution TEM images testify CNTs with different number of walls (Fig. 3b-d). Besides MWNTs, the samples obtained with Co–Mo/MgO and Fe–Mo/MgO catalysts demonstrate also bundles of single-walled CNTs (SWNTs) (Fig. 3b) and individual double-walled and triple-walled CNTs (Fig. 3c). The samples obtained with the Ni–Mo/MgO catalyst demonstrated MWNTs only (Fig. 3d). According to the statistical analysis of TEM images, the average outer diameter of CNTs is 7 nm, 8 nm, and 11 nm with the distribution of 4-10 nm, 4.5-12 nm, 6-16 nm for the samples obtained with Fe–Mo/MgO, Co–Mo/MgO, and Ni–Mo/MgO catalysts, respectively. The specific surface areas of the samples obtained with Co–Mo/MgO and Ni–Mo/MgO are 435 m²/g and 247 m²/g, which correlates with the increase in the number of CNT walls.

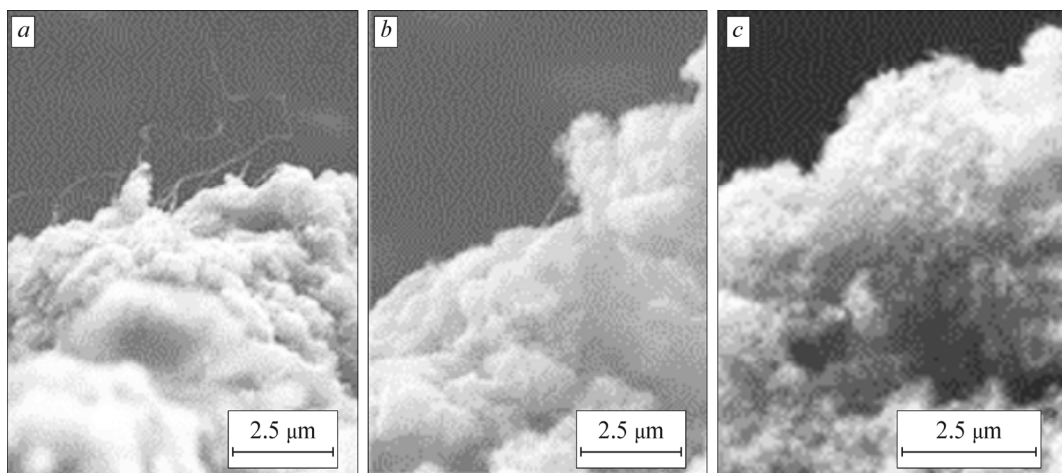


Fig. 2. SEM images of the samples obtained with Fe–Mo/MgO (a), Ni–Mo/MgO (b), and Co–Mo/MgO (c) catalysts.

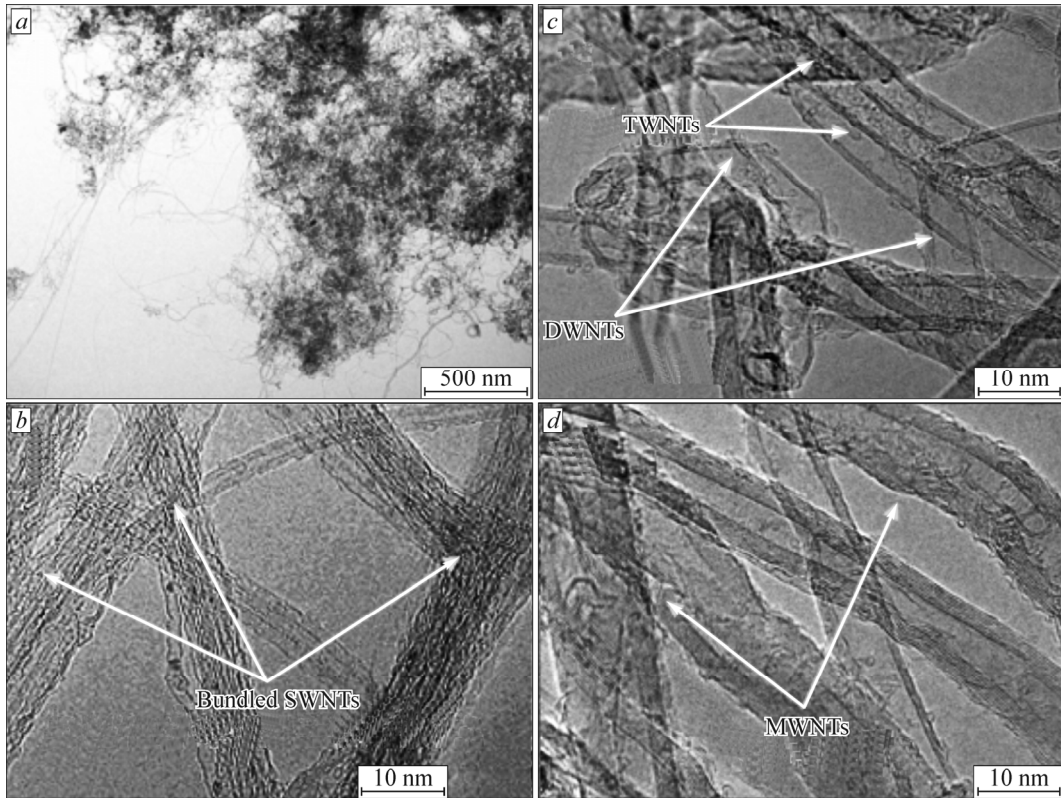


Fig. 3. Representative TEM images of CNTs obtained with the Co–Mo/MgO (overview image (a) and high-resolution image (b)), Fe–Mo/MgO (c), and Ni–Mo/MgO (d) catalysts. The arrows show bundles of single-walled CNTs (SWNTs), double-walled CNTs (DWNTs), triple-walled CNTs (TWNTs), and multi-walled CNTs (MWNTs).

According to the Raman spectroscopy data, the structure of the samples obtained with Fe–Mo/MgO or Co–Mo/MgO catalysts differs from the structure of the sample obtained with Ni–Mo/MgO (Fig. 4a). All spectra contained peaks typical of graphite materials: the D -band at $\sim 1355 \text{ cm}^{-1}$ corresponding to the vibrations of carbon atoms in disordered areas, the G -band at $\sim 1570 \text{ cm}^{-1}$ corresponding to the vibrations of carbon atoms in the graphene plane, and the $2D$ -band at $\sim 2700 \text{ cm}^{-1}$, which is the overtone of the D -band [23, 24]. The ratios of integral intensities of D - and G -bands (I_D/I_G) and $2D$ and G bands (I_{2D}/I_G) are used to estimate the defectiveness of carbon materials [25]. Calculated I_D/I_G and I_{2D}/I_G values increase in the row of $\text{Fe} < \text{Co} < \text{Ni}$ (Fig. 4b) to indicate higher density of defects for larger average CNT diameters. It was shown in [26] that the ratio I_{2D}/I_G depends on the diameter of MWNTs and grows together with the average diameter of MWNTs. The Raman

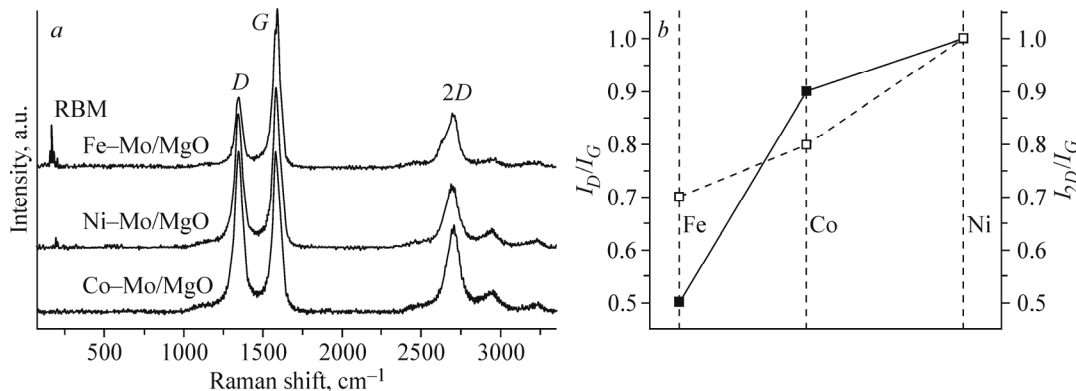


Fig. 4. Raman spectra (a) and integrated intensities I_D/I_G and I_{2D}/I_G (b) for the samples obtained with Fe–Mo/MgO, Ni–Mo/MgO, and Co–Mo/MgO catalysts.

spectra of the samples obtained with Fe–Mo/MgO and Co–Mo/MgO catalysts demonstrate radial breathing modes (RBM) of SWNTs. It is known that position of the RBM signal can be used to estimate the inner CNT diameter, however, it will differ notably from the value determined by statistical processing of TEM micrographs obtained for CNTs with the diameter larger than 3 nm [27].

NEXAFS spectroscopy is widely used to study structural features of carbon materials. Fig. 5 shows C K-edge spectra of carbon materials obtained with Co–Mo/MgO and Ni–Mo/MgO catalysts. Both spectra demonstrate resonances at 285.4 eV and 291 eV corresponding to $1s \rightarrow \pi^*$ and $1s \rightarrow \sigma^*$ transitions. The peak at 288.7 eV is assigned to the carbon atom covalently bound to the oxygen atom [28]. According to the XPS data, the surface oxygen content was 3% (Co–Mo/MgO) and 4% (Ni–Mo/MgO). The difference between these values cannot explain the fact that the sample obtained with Ni–Mo/MgO demonstrates much higher intensity of its spectrum at 287–289 eV. According to the Raman spectroscopy data, defective carbon areas may also contribute to this spectral region.

Electrochemical properties. The CV curves of the samples recorded with the scan rate of 5 mV/s demonstrate a close to rectangular shape (Fig. 6a) typical of double layer capacities of carbon materials. The peaks at 460–480 mV on the charge curve and at 200 mV on the discharge curve correspond to the redox processes responsible for the pseudocapacitance of the electrode. Presumably, these peaks are associated with Mo^{+6} reduction into intermediate oxides MoO_x ($2.5 < x < 3$) [29]. After the product of the synthesis is treated with a dilute HCl, molybdenum-containing nanoparticles are only left inside CNTs. The CNT walls can be etched during the cycling [30] to make molybdenum atoms accessible to electrolyte ions. Note that CV curves in Fig. 6a were recorded after 30 charge-discharge cycles at a scan rate of 200 mV/s.

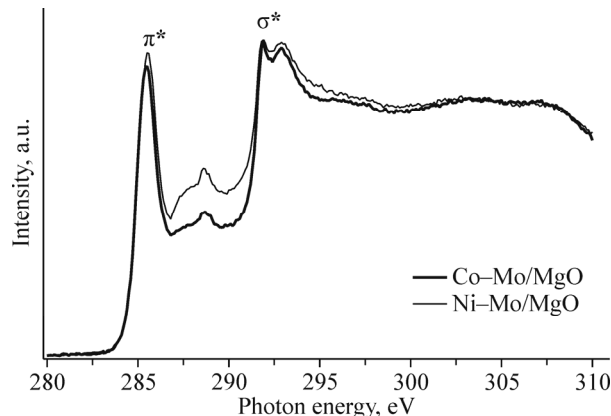


Fig. 5. C K-edge NEXAFS spectra of carbon materials obtained with Co–Mo/MgO and Ni–Mo/MgO catalysts.

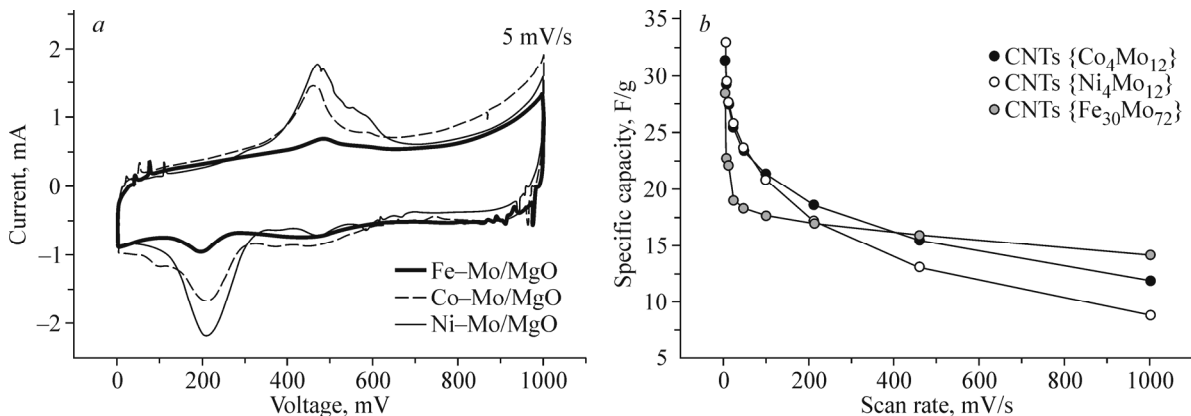


Fig. 6. CV curves of carbon materials at a scan rate of 5 mV/s (after 30 charge-discharge cycles) (a) and specific capacitance of the supercapacitor as a function of the scan rate (b).

As the scan rate grows, the specific capacitance of carbon materials decreases (Fig. 6b) due to smaller time for the diffusion of electrolyte ions between the particles, and becomes proportional to the specific surface area of the electrode material. When the supercapacitors based on CNT electrodes obtained with Co–Mo/MgO and Ni–Mo/MgO catalysts are recharged rapidly, their electrochemical capacitance correlates with the surface areas of these materials and increases in the row of Ni < Co < Fe. This increase is facilitated by strong electrical coupling of the material due to single- and double-walled CNTs in the samples. According to Raman spectroscopy data, the samples grown with Fe–Mo/MgO and Co–Mo/MgO catalysts demonstrate RBM peaks corresponding to the presence of single-walled CNTs responsible for the large specific capacitance at high scan rates. The high intensity of RBM peaks can be indirect indication of SWNT presence in the samples manifested in the values of specific capacitance of the electrodes at high scan rates. Since the electrochemical capacitance is substantially affected at low scan rates by redox reactions with participation of Mo and by the size and volume of the pores of the electrode material, it is subject to substantial change, namely the increase in the row of Fe < Co < Ni.

CONCLUSIONS

Polyoxomolybdates of Fe, Ni, and Co deposited on MgO were used as a source of catalytic nanoparticles during a CCVD synthesis of CNTs. The catalysts were activated by thermal decomposition of the clusters at 700 °C and subsequent gradual heating from ambient temperature to 900 °C in the flow of CH₄/H₂ gases. TEM images showed formation of CNTs with one to ten walls when using Fe–Mo/MgO and Co–Mo/MgO catalysts, and only MWNTs for the Ni–Mo/MgO catalyst. Raman and NEXAFS spectroscopy data and the measurements of specific surface area of the samples testify that CNTs obtained with the Fe–Mo/MgO catalyst demonstrate the most perfect structure and the smallest average diameter. The carbon materials were tested as supercapacitor electrodes. The study showed that the presence of single-walled and double-walled CNTs increases the electrode capacity at high scan rates. At low scan rates, the specific capacitance of CNTs is determined by the contribution from electrochemical reactions involving Mo which becomes accessible for electrolyte ions as a result of etching in defective and thin nanotube walls.

The NIIC team thanks Federal Agency for Scientific Organisations for funding. The authors acknowledge A. V. Ishchenko for TEM measurements, B. A. Kolesov for providing Raman spectra, and Helmholtz-Zentrum Berlin for Materials and Energy for the possibility of taking NEXAFS spectra within the framework of the Russian-German Laboratory.

The synthetic part of the study was supported by the PRC CNRS/RFBR program (grant No. 1023).

REFERENCES

1. A.-C. Dupuis. *Prog. Mater. Sci.*, **2005**, *50*, 929-961.
2. A. Moisala, A. G. Nasibulin, and E. I. Kauppinen. *J. Phys. Condens. Matter*, **2003**, *15*, S3011–S3035.
3. G. D. Nessim, A. J. Hart, J. S. Kim, D. Acquaviva, J. Oh, C. D. Morgan, M. Seita, J. S. Leib, and C. V. Thompson. *Nano Lett.*, **2008**, *8*, 3587-3593.
4. P. Chen, H.-B. Zhang, G.-D. Lin, Q. Hong, and K. R. Tsai. *Carbon*, **1997**, *35*, 1495-1501.
5. E. Flahaut, A. Peigney, C. Laurent, and A. Rousset. *J. Mater. Chem.*, **2000**, *10*, 249-252.
6. V. V. Chesnokov, V. I. Zaikovskii, and I. E. Soshnikov. *J. Phys. Chem. C*, **2007**, *111*, 7868-7874.
7. H. An, A. Kumamoto, H. Takezaki, S. Ohyama, Y. Qian, T. Inoue, Y. Ikuhara, S. Chiashi, R. Xiang, and S. Maruyama. *Nanoscale*, **2016**, *8*, 14523-14529.
8. W.-M. Yeoh, K.-Y. Lee, S.-P. Chai, K.-T. Lee, and A. R. Mohamed. *J. Alloys Compd.*, **2010**, *493*, 539-543.
9. Q. Zhang, Y. Liu, L. Hu, W. Qian, G. Luo, and F. Wei. *New Carbon Mater.*, **2008**, *23*, 319-325.
10. X. Xu, S. Huang, Z. Yang, C. Zou, J. Jiang, and Z. Shang. *Mater. Chem. Phys.*, **2011**, *127*, 379-384.
11. W.-M. Yeoh, K.-Y. Lee, S.-P. Chai, K.-T. Lee, and A. R. Mohamed. *New Carbon Mater.*, **2009**, *24*, 119-123.
12. F. Yang, X. Wang, D. Zhang, J. Yang, D. Luo, Z. Xu, J. Wei, J. Q. Wang, Z. Xu, F. Peng, X. Li, R. Li, Y. Li, M. Li,

- X. Bai, F. Ding, and Y. Li. *Nature*, **2014**, *510*, 522-524.
- 13. M. Kumar and Y. Ando. *J. Nanosci. Nanotechnol.*, **2010**, *10*, 3739-3758.
 - 14. G. D. Nessim. *Nanoscale*, **2010**, *2*, 1306-23.
 - 15. K. A. Shah and B. A. Tali. *Mater. Sci. Semicond. Process.*, **2016**, *41*, 67-82.
 - 16. A. R. Harutyunyan, B. K. Pradhan, U. J. Kim, G. Chen, and P. C. Eklund. *Nano Lett.*, **2002**, *2*, 525-530.
 - 17. E. Flahaut, R. Bacsa, A. Peigney, and C. Laurent. *Chem. Commun.*, **2003**, 1442/1443.
 - 18. G. Wang, L. Zhang, and J. Zhang. *Chem. Soc. Rev.*, **2012**, *41*, 797-828.
 - 19. A. Müller, C. Beugholt, P. Kögerler, H. Bögge, S. Bud'ko, and M. Luban. *Inorg. Chem.*, **2000**, *39*, 5176/5177.
 - 20. A. Müller, E. Krickemeyer, S. K. Das, P. Kögerler, S. Sarkar, H. Bögge, M. Schmidtmann, and S. Sarkar. *Angew. Chem. Int. Ed.*, **2000**, *39*, 1612-1614.
 - 21. E. V. Lobiak, E. V. Shlyakhova, L. G. Bulusheva, P. E. Plyusnin, Y. V. Shubin, and A. V. Okotrub. *J. Alloys Compd.*, **2015**, *621*, 351-356.
 - 22. E. V. Lobiak, E. V. Shlyakhova, A. V. Gusel'nikov, P. E. Plyusnin, Y. V. Shubin, A. V. Okotrub, and L. G. Bulusheva. *Phys. Stat. Sol. B*, **2018**, *255*, 1700274.
 - 23. M. S. Dresselhaus, G. Dresselhaus, R. Saito, and A. Jorio. *Phys. Rep.*, **2005**, *409*, 47-99.
 - 24. A. C. Ferrari and D. M. Basko. *Nat. Nanotechnol.*, **2013**, *8*, 1-26.
 - 25. E. F. Antunes, A. O. Lobo, E. J. Corat, and V. J. Trava-Airoldi. *Carbon*, **2007**, *45*, 913-921.
 - 26. V. L. Kuznetsov, S. N. Bokova-Sirosh, S. I. Moseenkov, A. V. Ishchenko, D. V. Krasnikov, M. A. Kazakova, A. I. Romanenko, E. N. Tkachev, and E. D. Obraztsova. *Phys. Stat. Sol. B*, **2014**, *251*, 2444-2450.
 - 27. Y. H. Jeong, H. J. Kim, K. K. Jeong, S. Y. Park, M. H. Yang, and C. W. Lee. *J. Phys. Chem. B*, **2004**, *108*, 17695-17698.
 - 28. A. Kuznetsova, I. Popova, J. T. Yates, M. J. Bronikowski, C. B. Huffman, J. Liu, R. E. Smalley, H. H. Hwu, and J. G. Chen. *J. Am. Chem. Soc.*, **2001**, *123*, 10699-10704.
 - 29. M. V. Martínez-Huerta, J. L. Rodríguez, N. Tsiovaras, M. A. Peña, J. L. G. Fierro, and E. Pastor. *Chem. Mater.*, **2008**, *20*, 4249-4259.
 - 30. E. O. Fedorovskaya, L. G. Bulusheva, A. G. Kurenya, I. P. Asanov, N. A. Rudina, K. O. Funtov, I. S. Lyubutin, and A. V. Okotrub. *Electrochim. Acta*, **2014**, *139*, 165-172.